14 Disordered and Biological Soft Matter

M. Ackermann, C.M. Aegerter, F. Atzeni, P. Dagenais, D. Dreher,
A. Keller (till March 2018), F. Lanfranconi (till December 2017), A. Mallavalli, S. Puri,
S. Scheibler (Master student), L. Schertel , J. Schneider, L. Selvaggi,
T. Stöckli (Master student) and S. Urdy (till July 2017)

in collaboration with: Institute of Molecular Life Sciences (K. Basler, T. Aegerter-Wilmsen, L. Pelkmans, D. Brunner), ETH Zürich (P. Koumoutsakos), MPI für Planzenforschung Köln (R.S. Smith), University of Fribourg (A. Jazwinska), University of Bern (C. Kulemeier, S. Robinson), Biozentrum Basel (M. Affolter), University of Konstanz (G. Aubry, G. Maret), MPI für Selbstorganisation Göttingen (C.C. Maass), Deutsches Luft- und Raumfahrtzentrum (M. Sperl), Université Joseph Fourier Grenoble (S. Skipetrov), Université Paris Denis Diderot (F. Graner), Technion Haifa (E. Akkermans).

In the group of disordered and biological soft-matter, we are interested in the behaviour of disordered materials outside of equilibrium, where instabilities arise, which lead to emergent structures. In particular, we are currently studying three overarching themes: The first is concerned with light transport in disordered, multiple-scattering media, where we aim at understanding, controlling and using multiply scattered light. In terms of understanding, we are also studying fundamental properties of multiple-scattering transport, such as the influence of path-reciprocity and Mie-scattering in the context of Anderson localisation and photonic band gaps. On the side of controlling light transport, we are using wavefront shaping to structure the illumination behind turbid layers, effectively compensating the multiple scattering. This can then be used in creating microscopy techniques that are capable to image structures in turbid media. Such novel imaging techniques for instance come into play in the second class of problems we are interested in, namely the regulation of biological development via mechanical forces. This is studied in the growth of the Drosophila wing and its folds as well as in the regeneration of fins of the zebrafish. The control of developmental processes by mechanical forces is also studied less in the context of direct growth regulation, but more in the context of shaping three dimensional structures as a driver of morphogenesis. This is studied in detail in the process of dorsal closure in Drosophila embryos. In all of this, the mechanical characterization of the materials in question is of paramount importance and we are using novel force techniques at the appropriate force levels ranging from nano Newtons to micro Newtons. The third theme finally, which complements these biological systems, consists of physical model systems that are far outside of equilibrium, such as granular gases and foams. These are studied in diamagnetic levitation in order to obtain information on long time dynamics, which is otherwise masked by the effects of gravity. In this way, we can study the overall properties of instabilities in disordered non-equilibrium systems.

Last years progress in the subjects of light transport in photonic glasses, imaging in turbid media, as well as the study of elastic properties of biological materials, such as the cytoplasm of the Drosophila embryo, its wing imaginal disc, and the bending stiffness of the zebrafish caudal fin are discussed in detail below.

14.1 Near field effects in the light transport through photonic glasses

In the study of light transport in photonic glasses, several aspects of light scattering are of importance. The refractive index difference determines the scattering strength, which is however also influenced by the size of the scatterers by the appearance of resonances due to Mie-scattering. Finally, in densely packed samples, positional correlations between the particles are of importance and have to be considered as well. We have recently developed and tested an extension of the energy coherent potential approximation [1], which takes into account collective effects of the scatterer arrangement [2]. In the case of weakly scattering polystyrene particles, we have been able to show that the scattering strength and the effective refractive index describe the experimental findings well, including the resonant effects due to the size of the particles, which is comparable to the wavelength of light. This can be seen in Fig. 14.1, where the scattering strength of several samples is shown as a function of the particle size. In addition to our data, the theory also describes data from [3]. The scattering strength in these experiments was determined from the width of the coherent backscattering cone [4]. With a working theory as this, capable of describing light transport in dense high index materials, it becomes possible to design materials that come close to the transition point to Anderson localisation [5, 6].

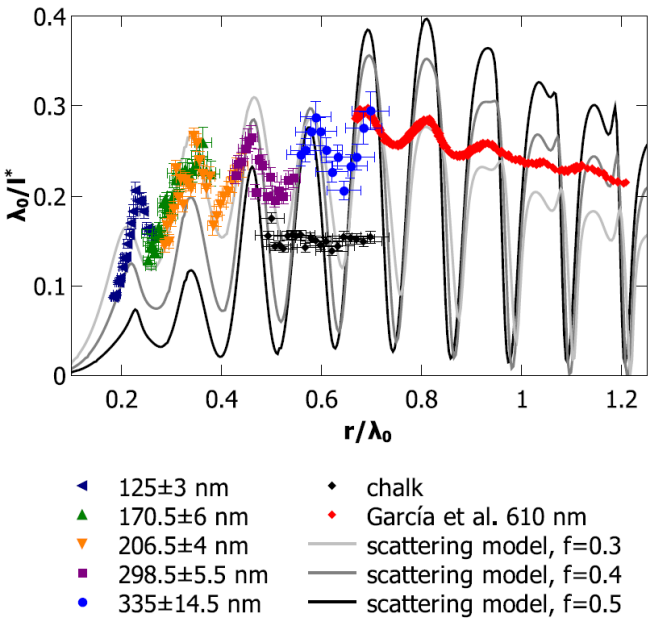

FIG. 14.1 – Scattering strength of photonic glasses made of almost mono-disperse polystyrene particles. Changing the wave-length of the scattered light, as well as the particle size, the full range of relative particle sizes can be studied and resonance effects due to Mie-scattering can be observed. The theoretical model describes our data, as well as those of García well, with a slight underestimation of the filling fraction.

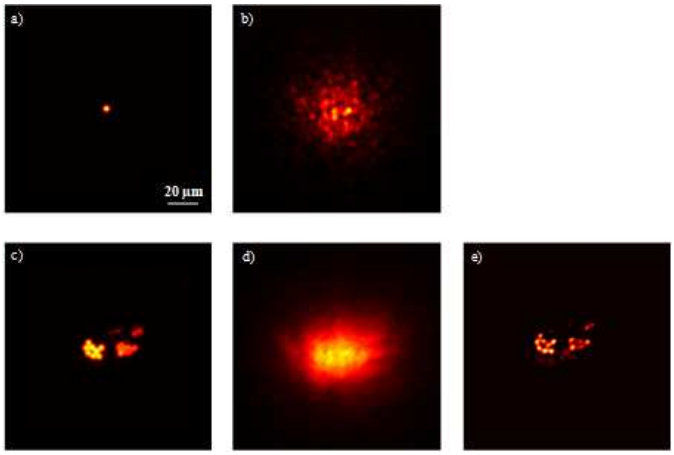

FIG. 14.2 – a) The image of a single fluorescent bead used as guide star. b) The same scene as in a) scrambled by the scattering layer indicating the PSF of the system. c) The image of a fluorescent scene. d) The same scene as in c) scrambled after passing the same part of the turbid medium. e) Reconstruction of the fluorescent scene seen in c) by deconvoluting image d) with image b) using blind deconvolution with 80 iterations. The distance between the fluorescent sample and the scattering medium was set to 5 mm.

[1] K. Busch and C.M. Soukoulis,
Phys. Rev. Lett. **75** 3445 (1995).

[2] G. Aubry, L. Schertel, M. Chen, H. Weyer, C. M. Aegerter, S. Polarz, H. Cölfen, and G Maret,
Phys. Rev. A **96** 043871 (2017).

[3] P. D. García, R. Sapienza, J. Bertolotti, M. D. Martín, A. Blanco, A. Altube, L. Vi na, D. S. Wiersma, and C. López, Phys. Rev. A **78**, 023823 (2008).

[4] S. Fiebig, C.M. Aegerter, W. Bührer, M. Störzer, G. Montambaux, E. Akkermans, and G. Maret,
Europhys. Lett. **81**, 64004 (2008).

[5] P.W. Anderson, Phys. Rev. **109**, 5 (1958).

[6] M. Störzer, P. Gross, C.M. Aegerter, and G. Maret,
Phys. Rev. Lett. **96**, 063904 (2006).

14.2 Deconvolution techniques for imaging in turbid media

In recent years, we have made great progress in controlling light transport through turbid media, developing fluorescence microscopy [7] in three dimensions [8], without direct optical access [9]. However in the context of structured illumination [10] and single plane illumination microscopy [11], which we have shown can work in a turbid environment, it can be of interest to determine the fluorescent structures via de-convolution techniques. This is of particular interest in biological situations, where the turbidity is detrimental to imaging, however not purely random. Here, we have recently adapted a method of using a guide star [12] for the determination of the point spread function (PSF) of the imaging system. As can be seen in Fig. 14.2, this works even in a situation where imaging is otherwise impossible [13]. This points a way apply to single plane illumination [11] in actual biological settings.

[7] I. M. Vellekoop and C.M. Aegerter,
Opt. Lett. **35**, 1245 (2010).

[8] G. Ghielmetti and C.M. Aegerter,
Opt. Express **20**, 3744 (2012).

[9] G. Ghielmetti and C.M. Aegerter,
Opt. Express **22**, 1981 (2014).

[10] A. Malavalli, M. Ackermann, C.M. Aegerter,
Opt. Express (2016).

[11] J. Schneider and C.M. Aegerter,
Journal of the European Optical Society **14**, 7 (2018).

[12] E. Edrei and G. Scarcelli,
Nature Scientific Reports **6**, 33558 (2016)

[13] J. Schneider and C.M. Aegerter
to be published (2018).

14.3 Determining the bending stiffness of live zebrafish fins

In the study of the influence of hydrodynamic forces on the growth and regeneration of zebrafish fins [14], we are studying how the fins are deformed during swimming and what forces are acting on these fins. This is in order to correlate the forces with growth patterns and growth rates that determine the size and structure of the zebrafish fins. For making the connection between deformation and forces quantitative, we need to determine the mechanical properties of live zebrafish fins, where the bony rays as well as the soft interray tissue is of interest. For this purpose, we have built a setup with which to determine the bending stiffness of the entire fin in a position dependent manner, see Fig. 14.3 [15]. With this, we can see that the bending stiffness of the fins is mainly determined by the bony rays, since a disruption of the interray tissue between the tissue does not influence the values for bending stiffness we obtain. The stiffness of the bones that we find is in good agreement with a scaled down value determined from the amputated rays bluegill sunfish [16], which are much larger than zebrafish and where the stiffness is therefore easier to determine. However, by bending only part of the fin, we are effectively stretching the interray tissue (see Fig. 14.4b) in addition to the bending. By cutting the tissue at the point of bending, we can separate these two contributions and hence obtain a determination of the effective elastic moduli of not only the bony rays, but also of the interray tissue, which is more than three orders of magnitude softer than the rays and is of the order of a few kPa.

[14] C. Pfefferli, and A. Jazwinska, Regeneration **2** 72 (2015).

[15] S. Puri, T. Aegerter-Wilmsen, A. Jazwinska, and C.M. Aegerter, Journal of experimental Biology **221**, 17077 (2018).

[16] B.E. Flammang, S. Alben, P.G.A. Madden, and G.V. Lauder, J. Morphol. **274**, 1044-1059 (2013).

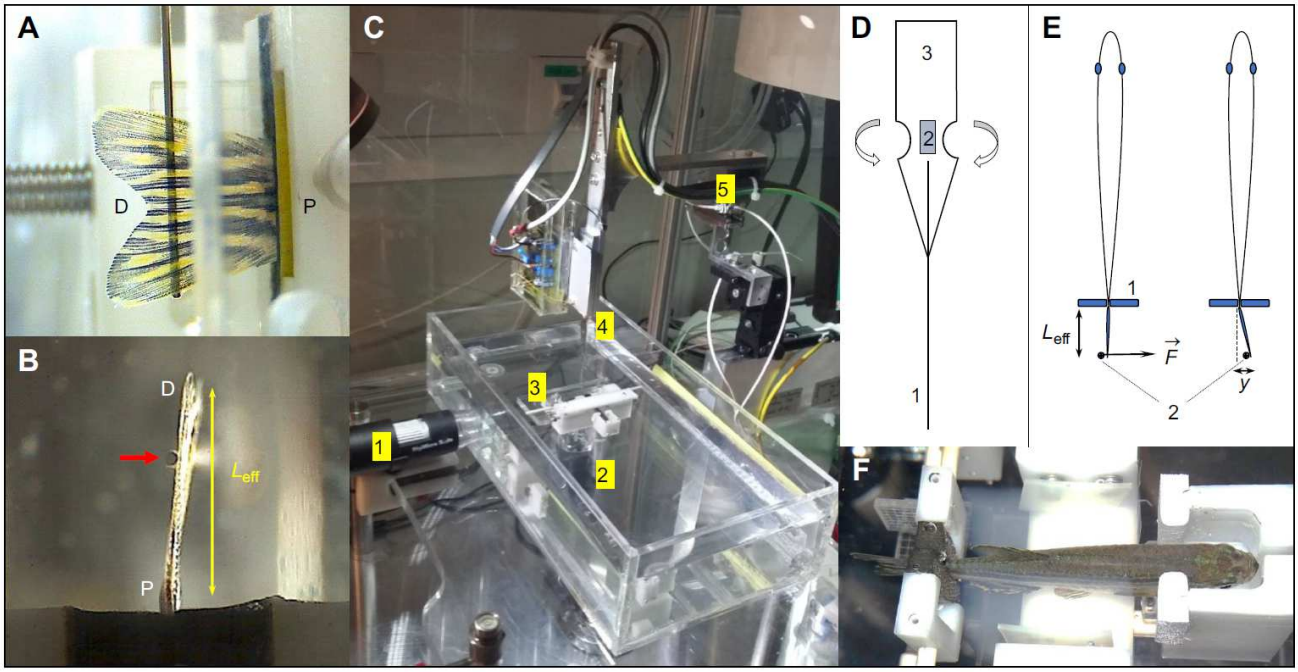

FIG. 14.3 – (A) Side-view of a lined force attack from the deflection pin onto the fin surface (D: distal end of the fin; P: proximal end of the fin). (B) Bottom-view showing the pin (red arrow) at a certain effective beam length from the fixation (black foam pads). (C) Overall impression of the measurement setup showing a water basin, two camera positions (1., 2.) as in (A) and (B) respectively, a fish holding device (3.) as also shown again in (F) and the sensor construct (4.) mounted onto piezo-based positioners (5.). (D) Design of the sensor construct with strain gages (2.) mounted onto a spring sheet (3.) together with the deflection pin (1.) that leads to the base of the strain gages to increase the effective bending moment together with the specialized geometry of the spring sheet (3.). (E) Measurement principle illustrating the deflection pin (2) applying a force at a certain proximal-distal position (effective beam length, Leff) leading to a certain displacement y. The fish peduncle is held by two opposing foam pads (1) as also shown in figure (B). (F) Zebrafish holding device showing an anesthetized adult specimen.

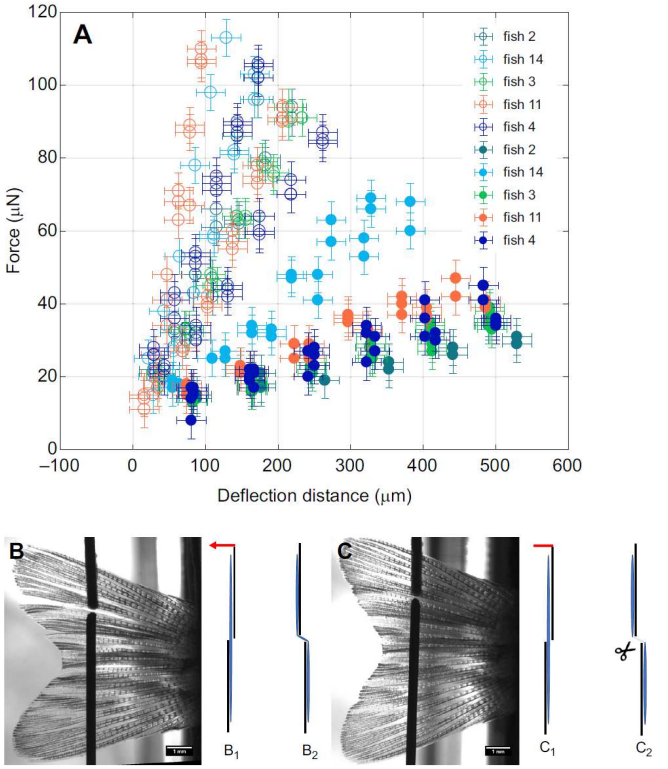

FIG. 14.4 – (A) The force extension curves for 5 fish are shown, while circled data points indicate measurements on intact tissues (B). At the same time data points (non-circled) are shown for surgically disrupted tissues (C), (error bars for deflection distance correspond to standard deviations (±20μm), equally for force (±5μN). Measurements were performed at the same positions in each fin, once between the 4th and 5th ray (B, C) and once between the 6th and 7th ray (not shown). The illustrations (B1, B2, C1, C2) represent front views. B1 and C1 represent the initial starting position, before a deflection (indicated by a red arrow) has occurred that would result in the configurations B2 and C2 respectively.

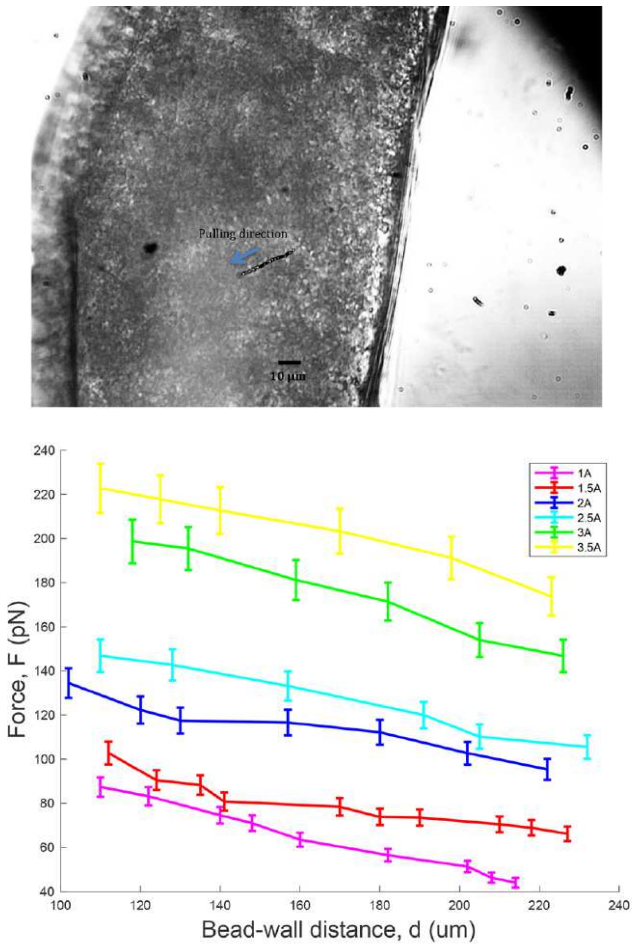

FIG. 14.5 – Top: Trace of a 2.8 μm bead pulled with a constant magnetic force inside a fly embryo. The field of view is 275 μm × 206 μm. Bottom: Force calibration curves of 2.8 μm Dynabeads for different current values.

14.4 Determining the viscoelastic properties of the cytoplasm in Drosophila embryos

In the context of morphogenesis, we are studying the process of dorsal closure in the Drosophila embryo [17]. Here, we are interested into how mechanical forces shape a tissue and actively lead to contractions [18]. For this purpose, the mechanical properties of tissues and cytoplasms in the Drosophila embryo. Given that we want to be able to actively apply forces and the scale of the forces present in embryos, we have built a magnetic tweezer setup [19], which is able to apply forces of the order of several hundred pico Newton onto super-paramagnetic beads that can be injected into the embryo at an early stage (see Fig. 14.5) and then positioned to a desired part of the embryo, such that they are incorporated into tissues of choice. With this, we have been able to determine the visco-elastic properties of the cytoplasm of mid-stage Drosophila embryos [19], where the viscous part is in reasonable agreement with a previous determination at the same stage of development that was done using passive microrheology [20].

[17] J. Solon, A. Kaya-Copur, J. Colombelli, D. Brunner, Cell **137**, 1331 (2009).

[18] T. Idema, J.O. Dubuis, L. Kang, M.L. Manning, P.C. Nelson, T. C. Lubensky, and A.J. Liu, PLoS One **8**, e77216 (2013).

[19] L. Selvaggi, L. Pasykarnakis, D. Brunner, and C.M. Aegerter, Review of Scientific Instruments **89** 045106 (2018).

[20] A.D. Wessel, M. Gumalla, J. Grosshans, and C.F. Schmidt, Biophys. J. **108**, 1899 (2015).

14.5 The influence of geometry on the elastic properties of the Drosophila wing imaginal disc

We have in the past extensively studied the mechano-regulation of growth in the Drosophila wing imaginal disc, where we have modelled the process [21, 22] and shown that mechanical feedback in growth regulation can lead to a size determination as well as uniform growth in the presence of growth factor gradients. In addition, we have shown that there are mechanical stresses present in the wing disc [23] and that mechanical tension can lead to an increase in cell division rates [24]. When studying these regulation mechanisms on a cellular level, the forces acting on individual cells need to be known even though the application of force is on the entire tissue level. Therefore, we have recently started to investigate how applied loads are distributed in the tissue and which parts of the tissue get stressed most. For this purpose, we have combined the stretching apparatus used previously [24] with a confocal microscope, such that the deformations of the tissue as well as the cells can be determined concurrently with the application of a mechanical load. This is shown in Fig. 14.6, where it can be seen that much of the initial elongation of the tissue is due to an unfolding of the corrugated structure.

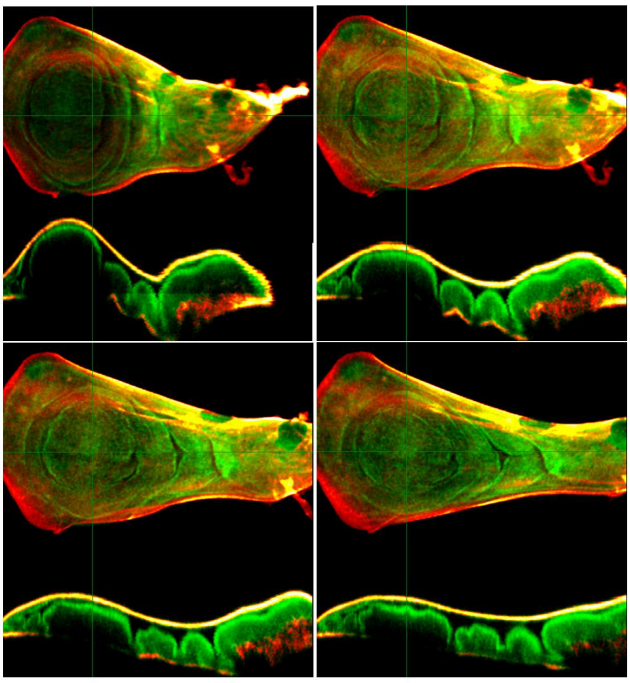

FIG. 14.6 – Deformation experiment, three-dimensional confocal microscopy images of 0 µm (top left), 30 µm (top right), 50 µm (bottom left) and 70 µm (bottom right) deformation of fixed boundary. The extracellular matrix is in red and the apical side of the tissue in green.

This leads to a strongly non-linear behaviour in the force-extension curve, shown in Fig. 14.7. After the unfolding, the extracellular matrix (ECM) surrounding the tissue (marked in red in Fig. 14.6) begins to experience the mechanical load. Since ECM is a dense network of collagen fibres, it is much stiffer than the rest of the tissue, such that its stretching requires more force, thus leading to an increase in the slope of the force extension curve. We have also modelled this computationally [25], where the non-linear response is reproduced reasonably well even using completely linear materials, see Fig. 14.7.

Thanks to the computational modelling, we can therefore now also have a picture of which parts of the tissue experience the most stress in a stretching experiments, such that the cellular mechanism can be investigated experimentally. This is shown in Fig. 14.8, where the deformation of the modelled wing disc is comparable to that of the experiment, but we in addition can determine the shear and normal stresses spatially resolved, showing that they are localised mostly in the ECM, as well as close to the folds.

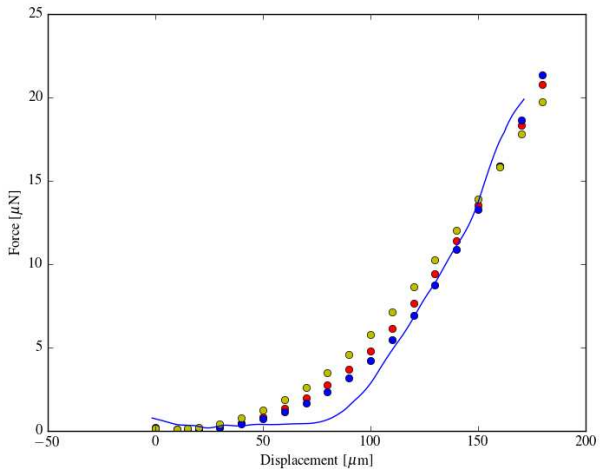

FIG. 14.7 – Solid line: Force extension curve averaged over nine subsequent extensions. The force extension curve is highly non-linear with a strong increase in its slope at an extension of roughly 80 µm, where the overall response stiffens by at least an order of magnitude. The fact that the extension returns to zero when the force is reduced indicates that the tissue reacts elastically on the time scale of the experiment, which is 900 s. The symbols show modelled force displacement curves with an overall elastic modulus of 1.1 kPa and an outside layer of ECM with a higher modulus by a factor of 50 (blue dots) and 100 (red dots). The yellow dots are as the red ones, but with additionally a harder layer on the apical side with a 100 times higher modulus than the entire wing disc.

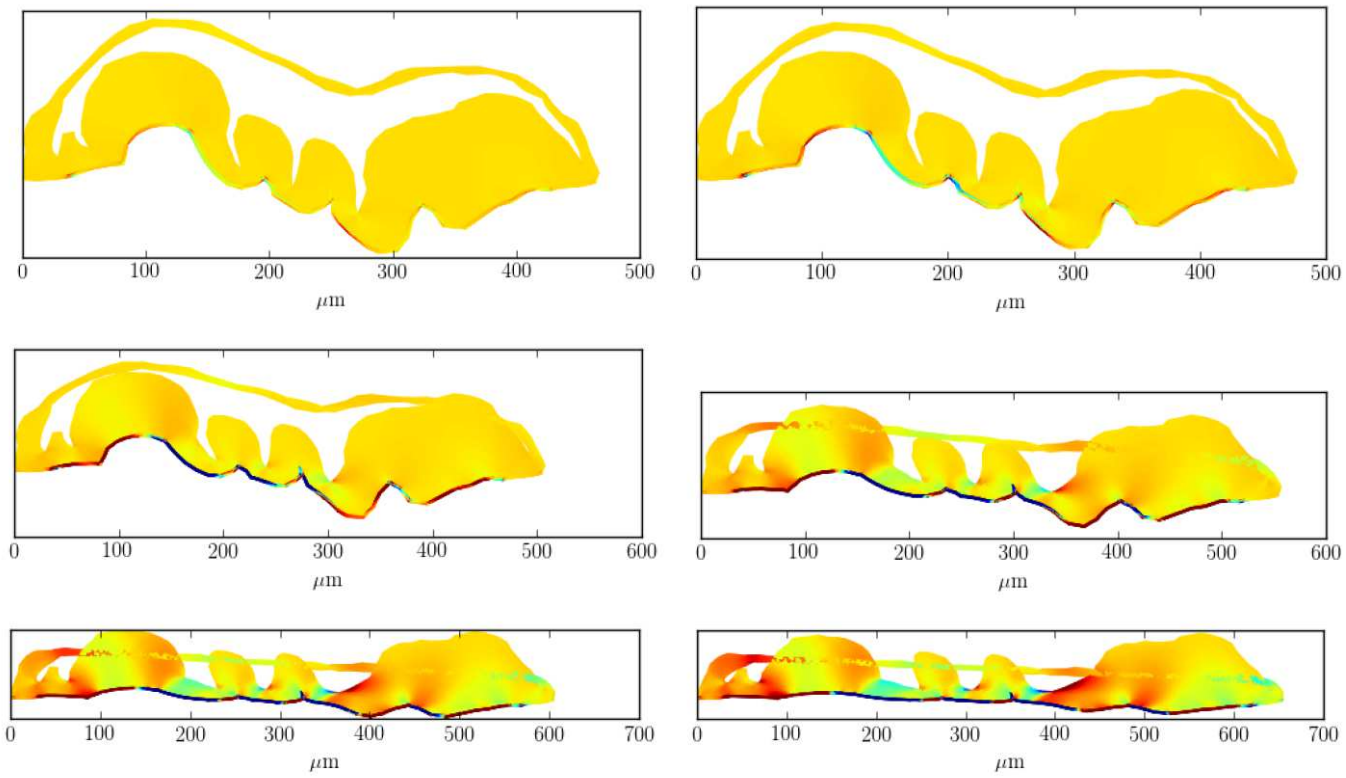

FIG. 14.8 – Modelled deformation history: color coded is the shear component σ_{xy} of the Cauchy stress tensor. The color scale varies from -0.03 MPa (blue) to 0.015 MPa (red).

[21] T. Aegerter-Wilmsen, C.M. Aegerter, E. Hafen, and K. Basler,
Mechanisms of Development **124**, 318 (2007).

[22] T. Aegerter-Wilmsen, M.B. Heimlicher, A.C. Smith, P. Barbier de Reuille, R.S. Smith, C.M. Aegerter, and K. Basler, Development **139** 3221 (2012).

[23] U. Nienhaus, T. Aegerter-Wilmsen, and C.M. Aegerter,
Mechanisms of Development **126**, 942 (2009).

[24] T. Schluck, U. Nienhaus, T. Aegerter-Wilmsen, and C.M. Aegerter,
PLoS One **8**, e76171 (2013).

[25] A. Keller, F. Lanfranconi, and C.M. Aegerter,
to be published (2018).